A Quantitative Analysis of Contractility in Active Cytoskeletal Protein Networks

Poul M. Bendix,*† Gijsje H. Koenderink,*‡ Damien Cuvelier,* Zvonimir Dogic,¶§ Bernard N. Koeleman,* William M. Brieher,‖ Christine M. Field,‖ L. Mahadevan,* and David A. Weitz*

*School of Engineering and Applied Sciences, Harvard University, Cambridge, Massachusetts; †Niels Bohr Institute, University of Copenhagen, Copenhagen, Denmark; ‡Foundation for Fundamental Research on Matter Institute for Atomic and Molecular Physics, Amsterdam, The Netherlands; ¶Rowland Institute at Harvard, Harvard University, Cambridge, Massachusetts; §Brandeis University, Waltham, Massachusetts; and ‖Department of Systems Biology, Harvard Medical School, Boston, Massachusetts

ABSTRACT Cells actively produce contractile forces for a variety of processes including cytokinesis and motility. Contractility is known to rely on myosin II motors which convert chemical energy from ATP hydrolysis into forces on actin filaments. However, the basic physical principles of cell contractility remain poorly understood. We reconstitute contractility in a simplified model system of purified F-actin, muscle myosin II motors, and α-actinin cross-linkers. We show that contractility occurs above a threshold motor concentration and within a window of cross-linker concentrations. We also quantify the pore size of the bundled networks and find contractility to occur at a critical distance between the bundles. We propose a simple mechanism of contraction based on myosin filaments pulling neighboring bundles together into an aggregated structure. Observations of this reconstituted system in both bulk and low-dimensional geometries show that the contracting gels pull on and deform their surface with a contractile force of $\sim$1 μN, or $\sim$100 pN per F-actin bundle. Cytoplasmic extracts contracting in identical environments show a similar behavior and dependence on myosin as the reconstituted system. Our results suggest that cellular contractility can be sensitively regulated by tuning the (local) activity of molecular motors and the cross-linker density and binding affinity.

INTRODUCTION

Contractile forces are essential for a number of cellular processes involving cell shape changes in the context of such phenomena as cell motility (1,2), cytokinesis (3), and tissue morphogenesis (4). These forces are transmitted by the cytoskeleton—a dynamic scaffold of interconnected protein filaments that spans the cytoplasm and is tethered to the plasma membrane. Actin and myosin II have been identified as key components in this contractile machinery. Filamentous F-actin provides the structural scaffold upon which the myosin motors move, powered by hydrolysis of ATP. While myosin II motors are nonprocessive, they organize into multimeric assemblies that are able to generate sustained gliding of actin filaments past one another (5–7). Cells control the motor activity and the assembly of actin and myosin both spatially and temporally. Under certain conditions, localized contractile structures are assembled, such as stress fibers in cells on flat substrates (8–10) and the contractile ring during cytokinesis (11,12).

Several recent studies have tried to model the contractile actin cortex using continuum hydrodynamics theories (13), considering the actin cytoskeleton as an active polar gel driven out of equilibrium by the hydrolysis of ATP. These hydrodynamic approaches predict the formation of complex patterns in actin-myosin gels such as asters and ringlike structures (14), which have been recently confirmed by in vitro experimental studies (15,16). Despite this success, there is still a limited understanding of the dependence of contractility and pattern formation in actin-myosin gels on microscopic parameters such as the number, activity, and processivity of the myosin motors or the local cross-linker density and actin network connectivity.

Experiments with various cytoplasmic extracts have shown that contraction is actin- and myosin-dependent and is accelerated by proteins that cross-link actin filaments (17–20). However, extracts are still complex multicomponent systems, and a systematic and quantitative study of mechanisms of contraction is difficult. For this reason, contraction has also been investigated in simplified reconstituted systems of purified cytoskeletal proteins. Starting in the 1940s (21), experiments on purified actomyosin solutions reported contraction or superprecipitation (22–24). These studies showed in particular that contraction of F-actin networks by myosin II at physiological ATP concentrations requires the presence of an F-actin cross-linker such as filamin A (25–27) or fascin (28). Recent theoretical work confirms that myosin motors are not capable of generating sufficiently large forces in cellular structures without actin filaments being cross-linked (29).

In this article, we focus on the dependence of contractility on α-actinin, a widely expressed protein that is particularly prominent in contractile cytoskeletal assemblies such as muscle myofibrils (30), stress fibers (8), and the contractile ring (11). We study contractility in a model-reconstituted system of purified actin, myosin, and α-actinin. We use calcium-insensitive α-actinin from chicken gizzard and chicken skeletal muscle myosin II, which is assembled into processive

Submitted July 24, 2007, and accepted for publication December 6, 2007.

Address reprint requests to David A. Weitz, Tel.: 617-496-2842; E-mail: weitz@seas.harvard.edu.

Editor: Elliot L. Elson.

0006-3495/08/04/3126/11 $2.00

doi: 10.1529/biophysj.107.117960

thick filaments. We image both the microstructure and the macroscopic behavior of the active network both early and late in the contractile event by using fluorescence confocal microscopy. The well-controlled nature of the model system allows us to systematically study the dependence of contractility on the number of cross-linkers and myosin motors per actin filament. We show that contractility requires a sufficiently high density of crossing bundles of actin filaments, which is obtained above a critical number of cross-linkers per actin filament. Based on this new insight and on microscopic images of the active networks, we propose that contractility is caused by myosin filaments pulling on neighboring bundles without significantly changing the dimensions of the bundles. Further, we quantify the macroscopic and microscopic contractile force as well as contraction velocity of the gels as a function of the myosin motor concentration.

We assess the biological relevance of our minimal system by performing similar experiments with concentrated cytoplasmic extracts from freshly laid *Xenopus* eggs. The extracts, termed M-phase or cytostatic factor (CSF)-arrested, are arrested in metaphase of meiosis II and are able to support and faithfully recapitulate many biological processes including spindle assembly and chromosome segregation (31). We place the extracts in similar geometries to facilitate comparison between contractile behavior of the reconstituted system and the cytoplasmic extract. We observe no contractility after inhibiting or depleting the myosin motors, which proves that myosin is responsible for the active properties of the gels. Our results shed light on the molecular mechanisms underlying macroscopic force generation by a collection of myosin motors embedded in a random network of actin filaments. Finally, we discuss implications of our findings for the regulation of contractility in cells.

MATERIALS AND METHODS

Protein purification

Actin was purified from rabbit skeletal muscle (32). Myosin II motor protein was isolated from chicken skeletal muscle (33) and stored in high ionic strength buffer (50% glycerol, 0.6 M KCl, 1 mM DTT, 50 mM phosphate, pH = 6.3) at −20°C. In all experiments we used myosin that was freshly dialyzed against a high ionic strength AB300 buffer (300 mM KCl, 4 mM $MgCl_2$, 1 mM DTT, 25 mM imidazole, pH 7.4) for 4 h, and clarified by ultracentrifugation for 10 min at 100 kRPM (Optima TLX Ultracentrifuge, Beckman Coulter, Fullerton, CA). Dialyzed myosin was stored on ice and used within three days after dialysis. The α-actinin cross-linker protein was purified from chicken gizzard (34).

Sample preparation

Samples were prepared under final buffer conditions of 25 mM imidazole, 50 mM KCl, 5 mM MgATP, 0.7 mM $MgCl_2$, and 0.2 mM $CaCl_2$, pH 7.4, which ensures optimum myosin ATPase activity. Myosin thick filaments assembled under these conditions consist of ~300 myosin molecules (35). The high ATP concentration prevents ATP depletion and concurrent myosin rigor binding on timescales of 4 h that exceed the timescale of our experiments (≤1 h). All buffers were mixed before adding myosin, α-actinin, and finally G-actin. Myosin and α-actinin concentrations were varied while the actin concentration was fixed at 23.8 μM. Inhibition of myosin II motor activity was attained by addition of blebbistatin (cat. No. B592490, Toronto Research Chemicals, North York, Ontario, Canada). In particle image velocimetry (PIV) experiments, yellow-dyed, carboxylated latex beads with a diameter of 3.024 μm (product No. 2FY-3000, Interfacial Dynamics, Eugene, OR) were added (50 μg/mL in sample) together with the buffers. The quality of the myosin motors was checked by performing motility assays with fluorescently-labeled actin filaments. From these experiments, the length of F-actin filaments was estimated to be ~5 μm. This number was confirmed by microrheology (36,37).

Cytoplasmic extracts

Concentrated M-phase extracts (*Xenopus*) were prepared from freshly laid *Xenopus laevis* eggs as previously described (31), with the following modification: no cytochalasin was added before the crushing spin. Briefly, eggs are washed in 5 mM Na-HEPES, (pH 7.8), 0.1 mM EDTA, 100 mM NaCl, 0.2 mM KCl, 0.1 mM $MgCl_2$ and 0.2 mM $CaCl_2$, then dejellied using 2% cysteine in 100 mM KCl, 1 mM $MgCl_2$, and 0.1 mM $CaCl_2$. The dejelly solution was removed and eggs washed several times in 10 mM HEPES (pH 7.7), 100 mM KCl, 1 mM $MgCl_2$, 0.1 mM $CaCl_2$, and 50 mM sucrose (XB buffer). The eggs were then crushed via centrifugation in XB buffer with 5 mM EGTA and 1 mM $MgCl_2$ (CSF-XB). Protease inhibitors were added before crushing. *Xenopus laevis* eggs are arrested in metaphase of meiosis II by cytostatic factor and are called CSF or M-phase extracts. A concentrated energy mix (150 mM creatine phosphate, 20 mM ATP, 2 mM EGTA, and 20 mM $MgCl_2$) was added at a dilution of 1:20 before freezing. Both fresh and frozen extracts were used with identical results. We prepared a high-speed supernatant (HSS) of M-phase extract by sedimenting the extract for 2 h at 50 K in a rotor (model No. TLS 55; Beckman Coulter), 112 K × g. This HSS is much reduced in protein concentration and such large particles as ribosomes, mitochondria, and vesicles. We found we could dilute M-phase extract 20-fold with HSS and still observe gel formation and contraction. Analysis of HSS via Western blots revealed substantial amounts of actin (~50% of the starting amount). Also, the extracts were observed to maintain their mitotic cell cycle state, as assayed by MPM2 antibody. Immuno-depletion of myosin II was performed as in Desai et al. (31) with minor modifications. In brief, protein-A Dynabeads (cat. No. 100-02, Dynal Biotech, Carlsbad, CA) were washed three times with TBST (tris-buffered saline Tween-20). Antibody was added to a 25-μL bead slurry (× 5 μL of beads), using either 1.5 μg of anti-myosin antibody or 3 μg of random rabbit antibody (cat. No. 011-00-003, Jackson Laboratories, Bar Harbor, ME). Tubes were placed at room temperature and rocked gently for 1 h. Beads were washed three times with 1/2 × CSF-XB (see above). After the final wash, all buffer was removed and 60 μL of extract was added to the beads. Tubes were kept on ice and mixed with frequent, gentle agitation for 1–2 h. Depleted extract was separated from the beads and its gelation/contraction properties were examined. The depleted and undepleted extracts were analyzed by SDS-PAGE and Western blot to determine the amount of protein reduction. Analysis of protein on the beads was carried out by SDS-PAGE; a prominent double band which cross-reacted with myosin-antibody was observed for the myosin beads with no similar bands observed in the control (by Coomassie stain or Western blot). The myosin II antibody was raised against a C-terminal peptide of *Xenopus* myosin II heavy chain (gift of Aaron Straight, Stanford University). Disruption of actin was done by adding cytochalasin D (1 μg/mL) or latrunculin A (0.5 μM) to the extracts before temperature shift.

Bulk contraction assay

Macroscopic contractility assays were performed using samples with a volume of 10 μL, which were deposited onto an inert oil layer (Fluorinert FC-40, 3M, St. Paul, MN; cat. No. F9755, Sigma, St. Louis, MO) on the bottom of a MatTek dish (model No. P35G-1.5-14-C, MatTek, Ashland, MA) equipped with a lid to minimize evaporation (Fig. 1 *A*). Network microstructures were

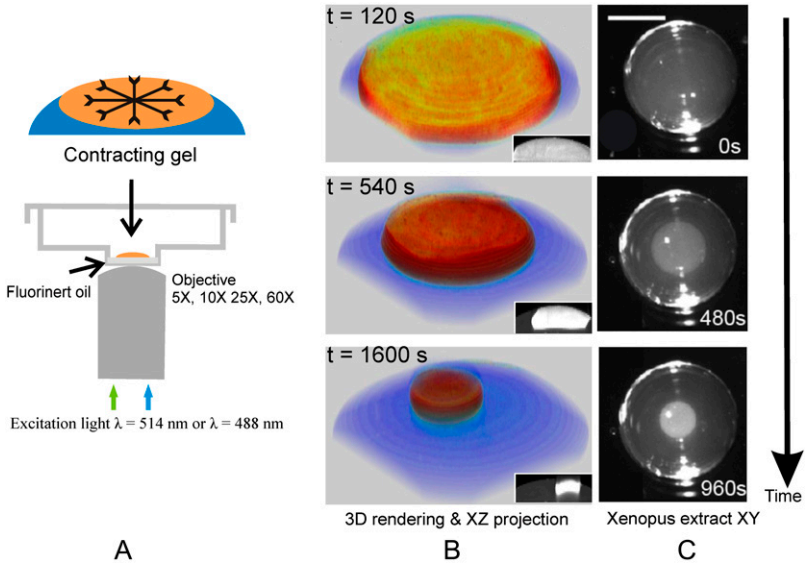

FIGURE 1 Contractile behavior of actin-myosin II networks cross-linked with α-actinin and of *Xenopus* cytoplasmic extracts in similar geometries. (*A*) Schematic illustration of contraction assay procedure. The sample was deposited onto an inert fluorocarbon oil layer in a dish with a recessed area in the center. The dish was closed by a lid to minimize evaporation. (*B*) Three-dimensional rendering of *XY*-confocal slices of the fluorescently labeled F-actin network (*orange*) contracting within the water droplet (*blue*). (*Inset*) Corresponding *XZ* projections through the gel (see also Fig. S1). The α-actinin to actin molar ratio is 0.11, and the myosin to actin molar ratio is 0.020 (see Movie S1). (*C*) Dark-field images of a contracting *Xenopus* extract which is placed within a layer of mineral oil. Bar, 400 μm.

observed on networks enclosed in chambers made of two cover glasses separated by a vacuum grease spacer. F-actin networks were fluorescently labeled with Alexa Fluor 488 phalloidin (Molecular Probes, Eugene, OR) with a [dye]/[actin] ratio of 1:2.5. In assays involving blebbistatin, actin was labeled with rhodamine phalloidin (Sigma Aldrich, St. Louis, MO), since blebbistatin is photoinactivated by blue light (38). We checked that varying the dye/actin ratio between 1:10 and 1:2 did not affect the occurrence or velocity of contraction. The networks were imaged on a confocal microscope (model No. LSM510, Carl Zeiss, Jena, Germany), using either a 60× NA 1.2 water immersion objective (~1-μm-thick optical sections) or a 5× objective (~40-μm-thick optical sections). An Argon laser was used for excitation at $\lambda = 488$ nm (for Alexa 488) and $\lambda = 514$ nm (for rhodamine); emission light was detected at $\lambda = 545$ nm and $\lambda = 560$ nm, respectively. The experiments were performed at ambient temperature, ~18°C. Contraction assays performed with *Xenopus* extracts were imaged using monochromatic light (λ = 480 nm) in a conventional binocular dissecting microscope and dark-field optics.

Capillary contraction assay

Macroscopic contraction assays with cytoplasmic extracts and reconstituted gels, respectively, were performed in bovine serum albumin (BSA) passivated capillaries of diameter $d = 400$ μm. The gels were suspended between two drops of mineral oil (cat. No. M-5904, Sigma).

Data analysis

Image analysis was done in MatLab 7.1 (The MathWorks, Natick, MA). The characteristic spacing between F-actin bundles was extracted from binary images, attained by thresholding with a threshold equal to the mean intensity plus one standard deviation of the corresponding image (39). Distances between on-pixels in binary images were recorded by scanning along pixel rows and columns. A *Z*-stack of 20 images separated by 1 μm was analyzed for each cross-linker concentration. Distributions of distances were least-square fitted to an exponential, $P = P_o e^{-(\xi/\xi_c)}$, with P_o and the decay length ξ_c as fitting parameters. Three-dimensional movies of contracting gels were rendered using *Z*-stacks of 20 image planes separated by 40 μm, which is roughly the focal depth for the 5× objective. Contraction velocities of active networks were measured both by tracking the rate of movement of the edge and by tracking embedded particles. PIV on tracer particles was performed using cross-correlation of 64 × 64 pixel size windows with 50% overlap. Subpixel accuracy was achieved by fitting a Gaussian to the cross-correlation peak function.

RESULTS

Macroscopic contraction of α-actinin cross-linked actin-myosin networks

To test the contractile activity of myosin II motors in filamentous F-actin networks, we perform macroscopic contraction assays. We place small droplets of sample (10 μL) containing a fixed concentration of fluorescently-labeled monomeric G-actin and varying concentrations of myosin II and α-actinin on a nonadsorbing oil layer. After 30 s, we image the time evolution of the homogenously formed F-actin network using confocal microscopy (Fig. 1 *A*). Initially, these networks are connected to the droplet surface. However, after ~5–10 min, the networks detach from the droplet surface and contract inwards. In a time period of ~30 min, the networks typically shrink to a final volume of only 5% of their initial volume. A typical example of this contraction process can be seen in Fig. 1 *B* (see also Supplementary Material Fig. S1 *B* and Movie S1), which shows three-dimensional reconstructions of an F-actin gel (shown in *orange*) contracting within a water droplet (shown in *blue*). Projections along the *XZ*-plane reveal that the gel contracts away from the nonadsorbing oil layer at the bottom surface but remains attached on top to the air interface, as shown in the insets of Fig. 1 *B* and Fig. S1 *C*. The networks thus contract into pancake-shaped gels.

To compare these observations with the behavior of cytoplasmic extracts, we perform similar contraction assays with extracts from *Xenopus* eggs. The extract is placed on top of a layer of nonadsorbing oil (Fig. 1 *C*) and imaged using dark-field optics. Upon heating from 4°C to 22°C, the extract forms a gel and subsequently contracts. During a time period

of 15–20 min, the extracts are observed to contract into small pancake-shaped gels, as seen in Fig. 1 *C*.

Contractility is controlled by the concentrations of motors and cross-linkers

Myosin-driven contractility of F-actin networks cross-linked with α-actinin depends on the concentrations of both the motors and the cross-linkers. At a fixed overall actin concentration of 23.8 μM, contraction only occurs at sufficiently high myosin concentrations and within a narrow window of α-actinin concentrations. This behavior is summarized in the state diagram in Fig. 2 *D*, where the crosses denote contractile networks while the open circles denote noncontractile networks. Macroscopic contraction occurs within the shaded region.

Myosin motor activity is essential for contraction. Contraction occurs only above a minimum myosin/actin molar ratio of 0.003, corresponding on average to 10 myosin II molecules per actin filament. Under the low salt conditions used, the functional units of myosin are thick filaments consisting of ~300 myosin molecules (35). The myosin concentration threshold for contraction is thus one myosin filament for every 30 actin filaments. To test that contraction is caused by mechanochemical activity of myosin, we inhibit the ATPase activity with blebbistatin, which slows phosphate release (40). Since myosin is affected by blebbistatin in its actin-detached state, blebbistatin addition does not lead to cross-linking of actin filaments by myosin. We find that 1 mM blebbistatin completely suppresses macroscopic contraction of samples prepared within the shaded contraction region in Fig. 2 *D*. We observe some residual activity in the form of local actin density variations, indicating that blebbistatin does not fully suppress myosin activity (Movie S2). Lower concentrations of blebbistatin are insufficient to suppress macroscopic network contraction.

Cross-linkers are also essential for contraction. In the absence of α-actinin, actin-myosin networks never contract, not even at the highest myosin concentrations used here (2.4 μM). In fact, the microstructure of actin-myosin II networks as observed with confocal microscopy (Fig. 3 *B*) is almost indistinguishable from that of pure F-actin networks (Fig. 3 *A*), apart from the occasional presence of small ($<$10 μm) dense actin clumps that are probably due to contamination with myosin rigor heads. The state diagram shows that contraction requires a minimum α-actinin/actin molar ratio of 0.05; or, on average, 90 α-actinin dimers per actin filament (Fig. 2 *D*).

At low concentrations of α-actinin, F-actin networks are weakly cross-linked and largely unbundled, apart from a few isolated F-actin bundles. The number of F-actin bundles increases as the [α-actinin]/[actin] ratio, $R_{\alpha:A}$, is raised (see Fig. 3 *C*). The network microstructure looks similar in the presence of myosin II thick filaments (Fig. 3 *D*). The myosin thick filaments do not contract the weakly cross-linked networks,

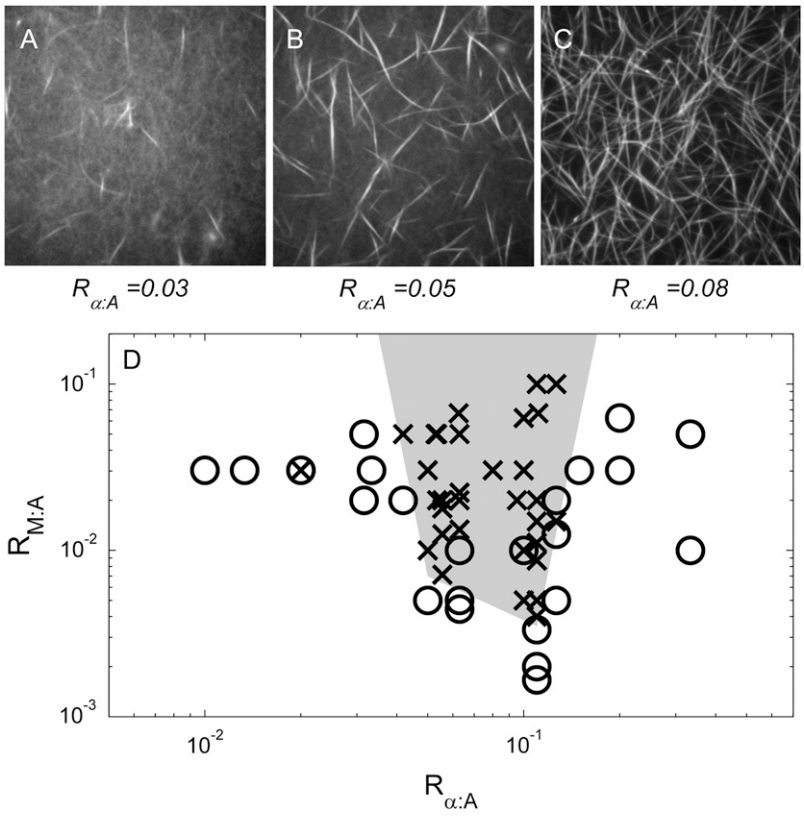

FIGURE 2 Contractility is sensitive to the concentrations of both cross-linkers and motors. (*A–C*) Microstructure of actin networks cross-linked with α-actinin, for three α-actinin concentrations. A Z-stack of 10 images, separated by 0.5 μm, was projected onto a single plane to visualize bundles that curve out of the focal plane. (*D*) State diagram showing the dependence of macroscopic contractility on the molar ratios of α-actinin cross-linkers and myosin II motors to actin, at a fixed actin concentration of 23.8 μM and filament length of ~5 μm. Crosses denote contracting networks; circles denote noncontractile networks. Outside the shaded region, at low myosin and α-actinin concentrations ($R_{M:A} < 0.003$, $R_{\alpha:A} < 0.04$) and at high α-actinin concentrations, there is no macroscopic contraction.

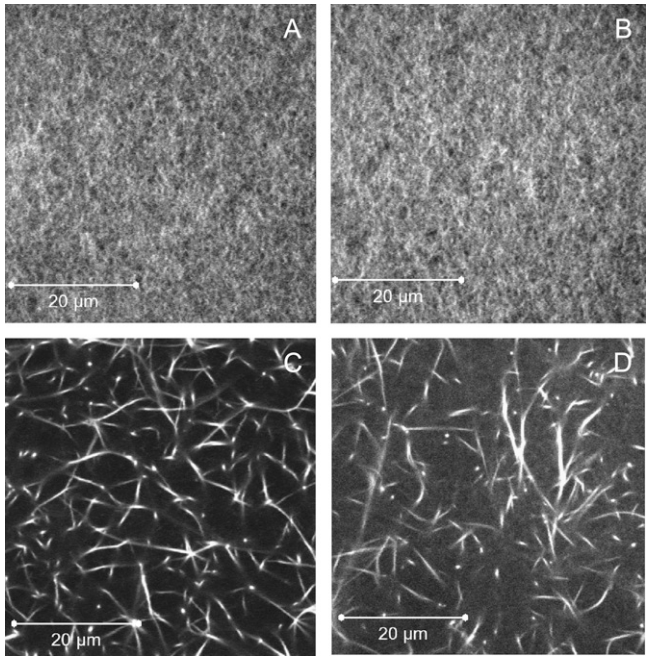

FIGURE 3 Confocal images of networks of fluorescently-labeled actin filaments (23.8 μM) in the presence of myosin II motors and/or α-actinin cross-linkers. (*A*) Entangled actin filaments. (*B*) F-actin-myosin II network, $R_{M:A} = 0.02$. (*C*) F-Actin network cross-linked with α-actinin, $R_{\alpha:A} = 0.063$. (*D*) F-actin network containing both myosin II thick filaments and α-actinin, $R_{\alpha:A} = 0.063$ and $R_{M:A} = 0.02$.

at least not on a timescale of 60 min. At $R_{\alpha:A}$ ratios above 0.05, virtually all actin filaments are assimilated into bundles that are connected and have an average spacing of 3 μm (Fig S2 and Fig. 2, *A–C*). The cross-linker threshold for bundle connectivity coincides with the threshold α-actinin concentration necessary to allow contraction by myosin II thick filaments (Fig. 2 *D*). This suggests that a minimal structure is necessary to propagate myosin-driven tension through the network. However, at high cross-link densities, $R_{\alpha:A}$ ratios >0.15, the bundled networks do not contract on the experimental timescale of 60 min, as indicated in Fig. 2 *D*.

Once again, we compare these results with observations of cytoplasmic extracts, by altering the network structure in *Xenopus* extracts by disruption of actin with cytochalasin D or latrunculin B. Adding either drug effectively inhibited contractility, confirming that contractility is dependent on an intact actin network structure.

The contraction velocity depends on the myosin motor concentration

The velocity of contraction measured by tracking the moving edge of a contracting network decays roughly exponentially in time. The velocity is initially high, typically 3–8 μm/s for the reconstituted F-actin gel, probably due to sudden release of elastic tension which has built up before the network detaches from the droplet surface. In the last stage of contraction, the edge velocity presumably becomes limited by the strongly decreasing pore size of the increasingly dense network (Fig. 4 *A*.)

To map spatial variations of the contraction velocity, we embed fluorescently labeled particles into the reconstituted networks that are larger than the average pore size and move with the network. We track these tracer particles during contraction using standard PIV (41), as illustrated in Fig. 5 *A*. In this particular example, contractility starts in the top-left corner, as indicated by the yellow arrows denoting the particle velocities. A diagonal velocity line scan across the image (indicated by *diagonal lines* in the *two images* in Fig. 5, *A* and *B*) shows that the particle velocities rapidly decrease from $\sim$2 μm/s at the edge to zero at a distance of $\sim$1 mm away (Fig. 5 *C*, *orange line*). As contraction progresses, the motions of the particles become more correlated throughout the gel in Fig. 5 *B*. The diagonal velocity line scan across this image shows a more uniform velocity distribution (Fig. 5 *C*, *blue line*).

The contractile rates for *Xenopus* extracts were found by tracking the edges as a function of time. The extracts initially contract at a rate of 1–2 μm/s, which decreases exponentially

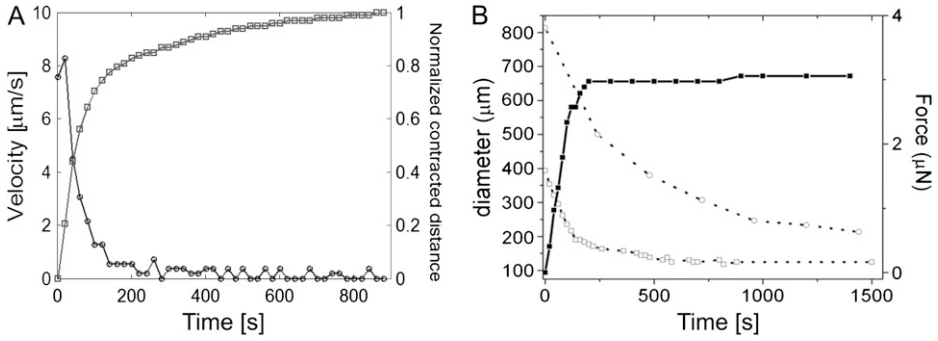

FIGURE 4 Temporal evolution of contracting gels measured by tracking the gel periphery. Typically the gels contract at a velocity of several microns per second during the initial phase. As the gels become denser, the velocity decays toward zero due to internal repulsion. (*A*) Velocity of periphery of reconstituted gel and corresponding normalized contracted distance as a function of time. $R_{\alpha:A} = 0.12$ and $R_{M:A} = 0.15$. (*B*) Temporal evolution of a cytoplasmic extract contracting in a drop geometry (*dotted line*, *open circle*) and in a capillary geometry (*dotted line*, *open square*), and the axial force generated on oil droplet in the capillary geometry (*straight line*, *closed square*).

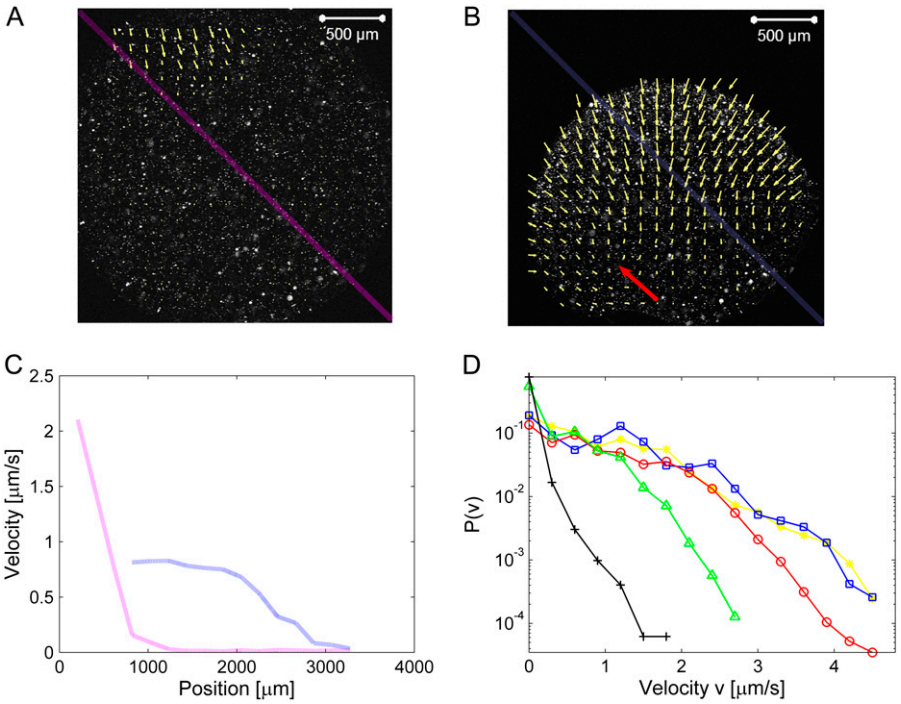

FIGURE 5 Contraction velocity of F-actin-myosin II networks probed with particle image velocimetry (PIV). (*A*) Large fluorescent particles with a diameter of 3 μm (*open dots*) embedded in the network act as discrete markers. Contracting gel ($R_{M:A} = 0.01$, $R_{\alpha:A} = 0.10$) initially shows local contractility near the air/water interface, but no large-scale dynamics ($t = 450$ s). Yellow arrows represent velocity vectors calculated from PIV analysis. Bar, 500 μm. (*B*) The same gel imaged at $t = 1156$ s shows correlated motion of the tracer particles toward a contracting center marked by the red arrow. Bar, 500 μm. (*C*) Velocity profiles obtained from diagonal line scans across the images. (*D*) Velocity distributions acquired during an entire contraction process for gels with varying myosin concentration and fixed concentrations of actin, 23.8 μM, and α-actinin, $R_{\alpha:A} = 0.10$. (*Squares*, $R_{M:A} = 0.100$; *asterisks*, $R_{M:A} = 0.050$; *circles*, $R_{M:A} = 0.025$; *triangles*, $R_{M:A} = 0.020$; and *plusses*, $R_{M:A} = 0.010$.) See Movie S3.

to 0.1 μm/s after ~15 min in a similar manner as in the reconstituted networks (Fig. 4 *B*). Contractility in *Xenopus* extracts can be significantly slowed down by reducing the number of active motors using an antibody directed against myosin II (Fig. 6 *A*). A reduction of the myosin concentration by a factor of two prolongs the duration of the contractile event by an order of magnitude (Fig. 6 *A*). An increase in waiting time before onset of contractility is also observed after successive dilutions of the extracts (Fig. 6 *B*).

The contraction velocity of the F-actin networks and the cytoplasmic extracts are always on the order of a micron per second, consistent with typical F-actin gliding velocities, ~3–4 μm/s, on dense layers of skeletal muscle myosin II immobilized on a surface (motility assays) (42). Moreover, the contraction velocities for both the reconstituted system and the cytoplasmic extracts depend on the myosin motor concentration, as shown in Fig. 5 *D* and Fig. 6 *A*. The distribution of the velocities of all embedded tracer particles during a contractile event shift to higher velocity values as the myosin concentration increases (Fig. 5 *D*). However, above a myosin/actin ratio of $R_{M:A} = 0.05$, the velocity distribution no longer changes appreciably, indicating that the contraction velocity saturates. These findings confirm that contraction is indeed an active process, driven by contractile activity of the myosin II thick filaments.

The contracting gels develop large contractile forces in the micronewton range

We measure the overall contractile force developed by the contracting gels by placing them in glass capillaries between two drops of mineral oil, as shown schematically in Fig. 7 *A*. The capillary walls are passivated with BSA, whereas the oil/water interface is highly sticky toward the gel. As a result, contractile gels pull away from the capillary wall but remain attached to the two oil/water interfaces, as shown in the sequence of images in Fig. 7 *B* and Movie S4. Gel contraction gradually deforms both oil/water interfaces and the oil droplets are pulled together. Above a certain force, the upper oil-droplet breaks, resulting in complete collapse of the gel into a dense mass.

The deformed shape of the oil/water interface during contraction reveals the magnitude of the contractile force. Using Laplace's Law, we can estimate the force from the change in interface curvature going from $1/R_i$ before contraction to $1/R_c$ during contraction:

$$\Delta P = 2\gamma\left(\frac{1}{R_c} - \frac{1}{R_i}\right). \quad (1)$$

In Eq. 1, ΔP is the change in Laplace pressure across the water/oil interface as the oil droplet deforms and γ is the surface tension of the oil/water interface which has been measured to ~4 mN/m (43). We measure the radii of curvature, on the side of the oil droplet facing the network, by locating the interface using image analysis and fitting a circle to it (Fig. S3 *A*). We find that the actively contracting gel pulls on the oil droplets with a force of ~1 μN just before the oil droplet breaks away. From the characteristic spacing between the F-actin bundles forming the contractile network, around ξ_c at ~ 4 μm, we estimate that this macroscopic force corresponds to an average force of ~100 pN per actin bundle. This

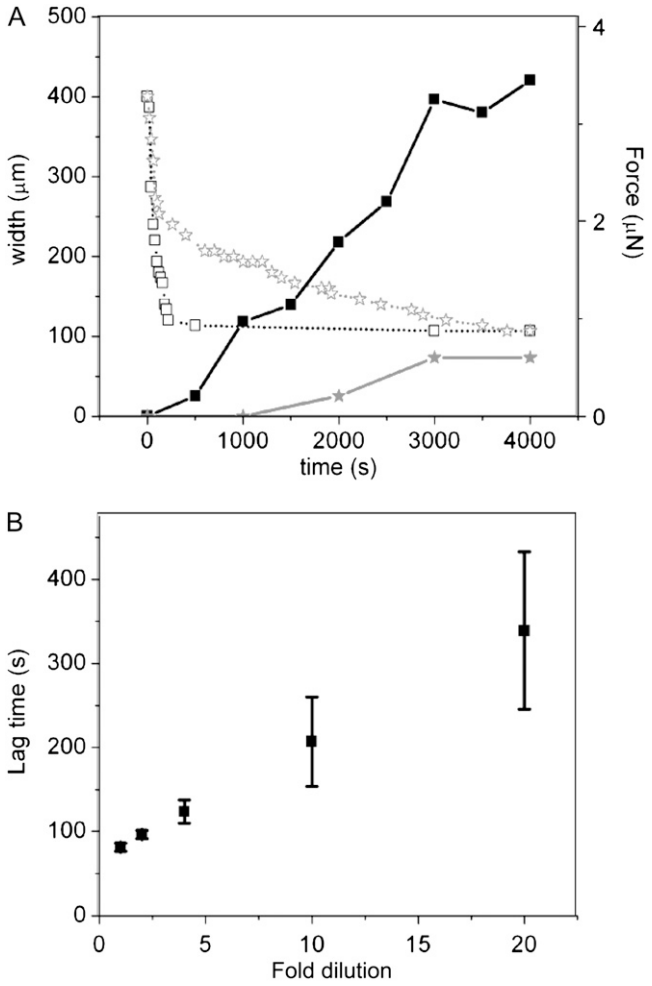

FIGURE 6 Influence of myosin II depletion on contraction dynamics measured for cytoplasmic extracts placed in capillaries. (*A*) (*Open squares*) Time evolution of gel diameter with no myosin depletion. (*Open stars*) Time evolution of gel diameter with myosin depleted. (*Solid squares*) Time evolution of the axial force exerted on the oil droplet with no myosin depletion. (*Solid stars*) Time evolution of the axial force exerted on the oil droplet with myosin depletion. (*B*) Effect of diluting the extract on the waiting time before onset of contraction.

value is likely an underestimation of the maximum forces that the network structure can sustain, since breakup of the oil droplet limits the maximum observable force.

Again, we compare this with the contractile behavior of extracts placed in capillaries, as shown in Fig. 7 *C*. The extract initially contracts radially inwards away from the BSA passivated glass surface and subsequently begins to pull in the axial direction, resulting in a gradual deformation of the sticky oil interface. From the change in curvature of the oil interface, we estimate the required force to deform the interface to be in the μN range. The *Xenopus* extracts were observed to break the oil droplet in a similar way as the reconstituted gels, but occasionally the extracts were observed to stop contracting before breakup of the oil droplet. This indicates that the maximum contractile force attainable with the extract is close to the measured force of 1 μN.

The network contracts by myosin filaments pulling bundles together

We observe changes in the microstructure of the network by imaging locally near the air/gel interface as the gel detaches from the interface (Fig. 8). Bundles at the air/gel interface are initially observed to stretch as they experience tension from the network interior (Fig. 8, *A* and *D*). Upon sudden detachment, the elastic energy stored in the network is released, and the network moves at high velocity away from the interface (Fig. 4 *A*, and Fig. 8, *B* and *E*). We observe bundles being transported toward the contractile center and becoming slightly more aligned orthogonal to the direction of movement (Fig. 8, *C* and *F*). Fig. 9 *A* and Movie S8 show a network of bundles moving to the left, whereas individual bundles always move orthogonally to their longitudinal orientation (*yellow arrows*). On very few occasions, we observe bundles buckling (Fig. 9, *B* and *C*) and thus, providing resistance against the contractile force.

We also image the network later when contraction has ceased. At the air/gel interface, a few bundles can be observed, some of which are still attached to the interface (Fig. 10 *A*). Between the air/water interface and the contracted gel, only few and isolated bundles can be seen, showing little loss of actin bundles during the contraction (Fig. 10 *B*). At the edge of the contracted gel, we observe bundles sticking radially outwards from the more densely contracted mass (Fig. 10 *C*). In most regions of the contracted gel, we cannot resolve any bundles, but in some less dense regions, closely packed bundles can be observed (Fig. 10 *D*). The bundles, which can still be optically resolved in the final contracted gel, have similar thicknesses compared to bundles imaged at an earlier stage in the contractile event (see Figs. S4 and S5). Instead, the bundles appear to become more densely packed in the final contracted state.

DISCUSSION

Contractility depends on the degree of network cross-linking

We demonstrate active myosin-driven contractility for reconstituted networks of actin filaments cross-linked and bundled with α-actinin. Since our model system contains only three, highly purified, components, we can quantify the requirements for contractility in terms of motor and cross-linker densities (at a fixed actin concentration of 23.8 μM).

We find that contractility requires a minimum α-actinin to actin ratio of 0.05, close to the onset cross-linker concentration for formation of connected networks of F-actin bundles (see Fig. 2, *A–C*, reported also elsewhere (44,45)). We propose that contractility requires a sufficiently connected net-

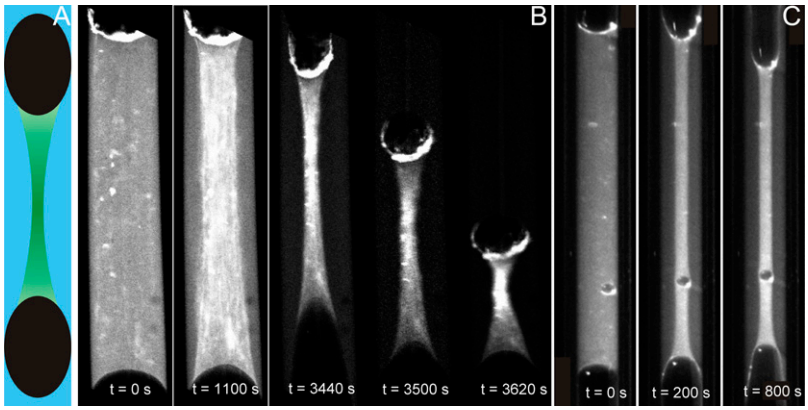

FIGURE 7 Measurement of contractile force developed by actin-myosin-α-actinin networks and *Xenopus* extracts contracting in identical capillaries. (*A*) Schematic of experimental setup. The gels are sandwiched between two oil droplets in BSA-passivated glass capillaries with an inner diameter of 400 μm. (*B*) Confocal images of the fluorescently-labeled network at five different time points. Initially the network pulls away from the capillary walls but remains attached to the oil droplets, which are gradually deformed as the gel contracts. Above a certain tension, one of the oil droplets breaks, allowing the gel to collapse completely. $R_{\alpha:A} = 0.11$ and $R_{M:A} = 0.10$. See Movie S4. (*C*) Dark-field images of a contracting cytoplasmic extract isolated from *Xenopus* eggs. The extract initially pulls away from the BSA-coated capillary wall but gradually deforms the oil droplets in much the same way as observed with the reconstituted gel in panel *B*.

work, which can transmit the contractile stresses generated by internal myosin motor activity. A few earlier articles describing reconstituted networks of actin, myosin II, and various cross-linkers also point out the necessity of cross-linking for contractility (25–28). Solutions of non-cross-linked actin filaments and myosin II mini-filaments indeed do not contract (16,46). We suspect that the superprecipitation phenomenon reported in older work with purified actomyosin (21–24) is caused by ATP depletion, residual actin-binding proteins, and/or inactive myosin rigor heads acting as cross-links. We find that macroscopic gel contraction is arrested at high cross-link densities, above α-actinin/actin ratios of 0.15. In this regime, most of the actin filaments are assembled into bundles and a further increase of the cross-linker concentration does not change the average bundle spacing (Fig. S2 *B*). Qualitatively similar observations were reported for a reconstituted system based on actin, smooth muscle myosin II, and filamin A cross-linkers (27).

Contraction is an active process driven by myosin motors

Contraction of cross-linked actin-myosin networks is mediated by internal stresses that are actively generated by the myosin motors. This conclusion is supported by several observations. First, inhibition of the motor ATPase activity with blebbistatin suppresses macroscopic contractility (Movie S2). Second, the shrinkage velocity of contracting gels is consistent with the translocation velocity of actin filaments measured in motility assays with skeletal muscle myosin II (42). The shrinkage velocity saturates when the myosin/actin ratio exceeds 0.05, or approximately three actin filaments per myosin filament (Fig. 5 *D*). This likely occurs because the myosin filaments have a similar length as the actin filaments, and each can bind to multiple actin filaments.

The contractile rates measured for *Xenopus* extracts were also consistent with velocities of single myosin motors and could likewise be modulated by changing the number of motors (Fig. 6). Also, the measured contractile velocities are similar to those measured for stress fibers in nonmuscle cells (47). Shrinkage velocities during contraction have previously been measured for bundles of F-actin filaments in vitro mixed with *Dictyostelium* myosin II and fragments of chicken skeletal muscle myosin II (48). The contractile velocities of 0.1–1 μm/s reported for these bundles were an order-of-magnitude slower than observed here, perhaps due to friction counteracting the filament sliding. Interestingly, this study reported not only contraction but also elongation of bundles. In contrast, we observe only contraction for (at least initially) disordered networks of actin. *Xenopus* extracts were likewise observed to contract rather than expand, which is consistent with findings reported previously that cytochalasin has to be added to CSF extracts to prevent contraction (31). It remains an interesting open question whether gels always exclusively contract, and if so, why. We speculate that symmetry breaking at the gel periphery plays a role. Contraction is always observed to start at the air/gel interface and then to progressively move inwards. This symmetry breaking likely occurs because F-actin bundles within the network are subject to isotropic tension, whereas peripheral bundles are subject to a large unbalanced tension from the bulk, exceeding the force required to detach the gel from the gel/air interface.

We did not investigate the polarities of the filaments in the bundles; in fact, such a measurement is complicated, given the high filament density within the bundle. Interestingly, in Meyer and Aebi (44), it is suggested, on the basis of electron microscopy studies, that α-actinin bundles F-actin in both parallel and antiparallel orientations, but with a slight preference for antiparallel bundling. Such a preference, if existing, might explain why α-actinin cross-linked networks contract more efficiently than networks bundled by biotin-streptavidin or filamin. A comparative study using different cross-linker types could delineate the effect of cross-linker geometry and binding affinities on contraction parameters like velocity and force.

Despite the initial presence of ATP in the polymerizing networks, we always observe contractile activity a few

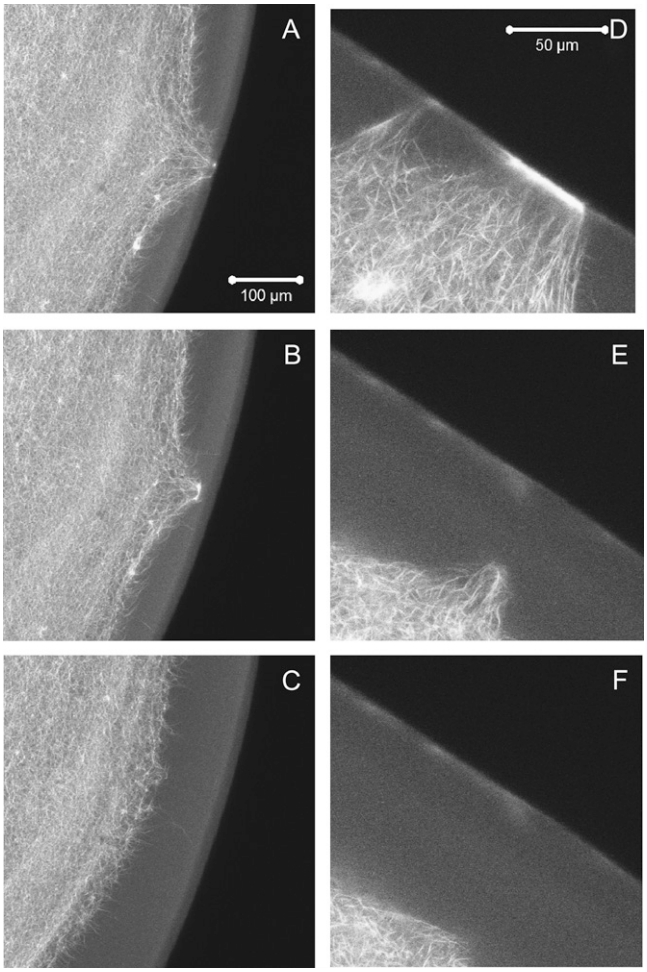

FIGURE 8 Network structure during the initial phase of the contractile event. Images show two separate events (*left* and *right columns*) at different magnification of bundles stretching at the interface and subsequent detachment from the interface. The weak attachment to the interface enables the network to initiate the contraction at the interface. (*Left* and *right columns*) Two different detachment events at two different magnifications. See Movies S6 and S7.

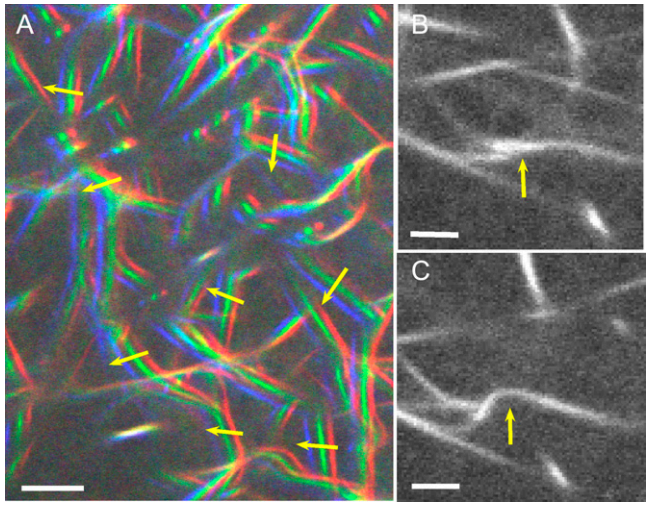

FIGURE 9 Movement of bundles during contraction in a region between the periphery and the center of the gel. (*A*) Three images of the same network captured at few-second intervals overlaid as red, green, and blue colors. The bundles in red correspond to the first image and the blue bundles correspond to the last image. Bar, 5 μm. (*B* and *C*) A rare event of buckling of a single bundle. The direction of buckling is orthogonal to the direction of network contraction. Yellow arrows indicate direction of movement of single bundles. Bar, 2 μm. See Movie S8.

minutes after formation of the networks. The early contractile networks do look similar to networks without myosin motors, indicating that the effect of the motors is to build up tension during the first minutes preceding contraction. We always added the G-actin last to achieve proper mixing of the proteins. However, an interesting future experiment could be to initially cage the ATP to study the formation of the network in presence of rigor binding motors, followed by uncaging of the ATP by UV-light and, consequently, activation of the motors (16).

During contraction, we observe no direct evidence of thickening of bundles (Fig. 9 *A* and Movie S8, Fig. S5). Instead, we observe bundles being transported while the pore size of the network gets smaller as the contraction proceeds. Contractility should be possible once the bundles are close enough for the myosin filaments to operate on crossing bundles. This implies that, at the threshold cross-linker concentration where the pore size of the network decreases dramatically and consequently the number of crossing bundles increases (Fig. S2 *B*), contractility should occur. Below this threshold concentration of cross-linkers, the bundles are too far apart, and consequently, no contractility is observed. If, however, contraction was mediated through shortening of bundles by actin filament sliding, we would expect to see an increase in the thickness of bundles. Also, we would expect isolated bundles observed in less cross-linked networks to become thicker. We did not observe significant shape changes of bundles and hence, do not expect filament gliding within the bundles to be the primary mechanism of contraction. However, this mechanism could permit contraction without thickening of bundles if there was room for interdigitation between antiparallel filaments within the bundles (27). Therefore, a quantitative analysis of the bundle intensities at different regions in the gel will be necessary to rule out this mechanism of contraction.

A simple model system for cytoplasmic contractility

Our purified model system, while being an oversimplification of a cell, has intriguing implications. In particular, our observations predict that regulation of motor activity and cross-linker density are powerful ways for controlling network contractility. Our experiments with *Xenopus* extracts indeed show that contractility can be regulated in a similar way by changing the ratio of myosin motors and cross-linkers relative

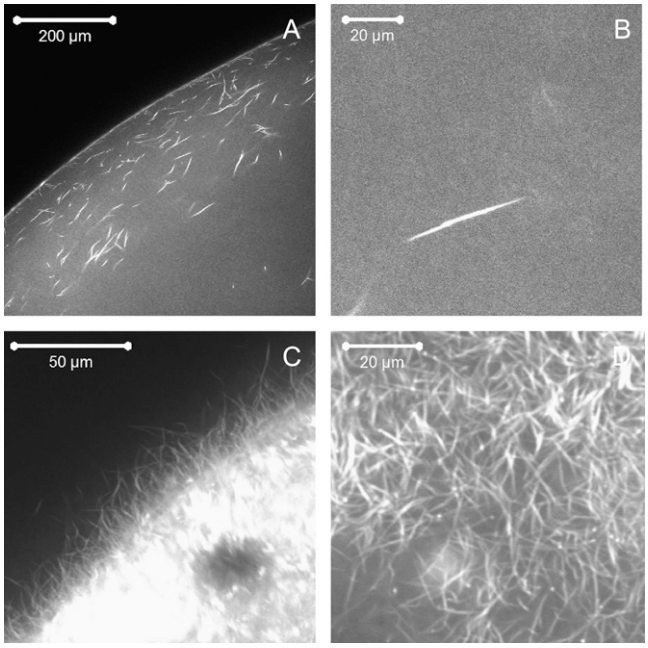

FIGURE 10 Images from different locations after the gel has contracted. (*A*) A few bundles are scattered near the air/gel interface, whereas others remain bound to the interface. (*B*) Only a few bundles are observed in the space between the air/gel interface and the contracted gel. (*C*) Bundles are seen sticking radially outwards from the surface of the contracted gel. (*D*) Bundles can be optically resolved in relatively less dense regions of the contracted gel.

to actin. Both the rate of contraction and the ability of an extract to exert mechanical forces on its surroundings are strongly reduced by depleting myosin (Fig. 6 *A*).

The purified networks develop contractile forces of $\sim 1\ \mu$N, corresponding to an average force of tens of piconewtons per F-actin bundle. The maximal forces generated by the *Xenopus* extracts were also measured to be $\sim 1\ \mu$N. These forces represent the force required to break the attachment to the gel interfaces, and do not necessarily correspond to the maximum forces the gels are able to generate. However, occasionally we observe a stalling behavior of the contracting extracts, indicating that the maximum attainable contractile force has been reached. Contractile processes in cells involve forces that span several orders of magnitude. The force developed during contractile ring progression is tens of nN in sea urchin eggs (49). Single keratocyte cells exert traction forces of tens of nN on a flat substrate (1,50). Fibroblasts develop even larger traction forces of $\sim 1\ \mu$N per cell, similar to the contractile forces measured here.

The ability of our minimal system to reproduce contractile behavior observed for cytoplasmic extracts shows that simple reconstituted systems can be used to model contractility in much more complex systems.

In conclusion, we have shown that contractility in actin-myosin networks can be regulated by modulating the network structure through the extent of cross-linking or through the concentration of myosin motors. Contractility was only observed within a narrow window of cross-linker concentrations, whereas a minimal concentration of myosin motors was required for contractility. Macroscopic contractile velocities were consistent with gliding velocities of single actin filaments gliding over myosin-coated flat surfaces. The contractile behavior of the reconstituted system strikingly resembled the contractile behavior observed for cytoplasmic extracts.

SUPPLEMENTARY MATERIAL

To view all of the supplemental files associated with this article, visit www.biophysj.org.

We thank Alexandre Kabla for fruitful discussions. The confocal microscope is maintained by the Harvard Center for Nanoscale Systems.

P.M.B. was supported by (Biomedical Optics and New Laser Systems) Risoe National Laboratory Denmark, the Danish Graduate School of Molecular Biophysics, and the Lundbeck Foundation, Denmark. G.H.K. was supported by a European Marie Curie grant (No. FP6-2002-Mobility-6B, No. 8526). C.M.F. was supported by National Institutes of Health grant No. GM23928. D.A.W. was supported by the Harvard Materials Research Science and Engineering Centers (grant No. DMR-0213805), National Science Foundation (grant No. DMR-0602684 and grant No. CTS-0505929), and National Science Foundation (grant No. DMR-0602684).

REFERENCES

1. Verkhovsky, A. B., T. M. Svitkina, and G. G. Borisy. 1999. Self-polarization and directional motility of cytoplasm. *Curr. Biol.* 9:11–20.
2. Medeiros, N. A., D. T. Burnette, and P. Forscher. 2006. Myosin II functions in actin-bundle turnover in neuronal growth cones. *Nat. Cell Biol.* 8:216–226.
3. Biron, D., E. Alvarez-Lacalle, T. Tlusty, and E. Moses. 2005. Molecular model of the contractile ring. *Phys. Rev. Lett.* 95:098102.
4. Franke, J. D., R. A. Montague, and D. P. Kiehard. 2005. Nonmuscle myosin II generates forces that transmit tension and drive contraction in multiple tissues during dorsal closure. *Curr. Biol.* 15:2208–2221.
5. Verkhovsky, A. B., and G. G. Borisy. 1993. Non-sarcomeric mode of myosin II organization in the fibroblast lamellum. *J. Cell Biol.* 123: 637–652.
6. Svitkina, T. M., A. B. Verkhovsky, K. M. McQuade, and G. G. Borisy. 1997. Analysis of the actin-myosin II system in fish epidermal keratocytes: mechanism of cell body translocation. *J. Cell Biol.* 139: 397–415.
7. Bridgman, P. C. 2002. Growth cones contain myosin II bipolar filament arrays. *Cell Motil. Cytoskeleton.* 52:91–96.
8. Edlund, M., M. A. Lotano, and C. A. Otey. 2001. Dynamics of α-actinin in focal adhesions and stress fibers visualized with α-actinin green fluorescent protein. *Cell Motil. Cytoskeleton.* 48:190–200.
9. Katoh, K., Y. Kano, M. Amano, H. Onishi, K. Kaibuchi, and K. Fujiwara. 2001. Rho-kinase mediated contraction of isolated stress fibers. *J. Cell Biol.* 153:569–583.
10. Kumar, S., I. Z. Maxwell, A. Heisterkamp, T. R. Polte, T. P. Lele, M. Salanga, E. Mazur, and D. E. Ingber. 2006. Viscoelastic retraction of single living stress fibers and its impact on cell shape, cytoskeletal organization, and extracellular matrix mechanics. *Biophys. J.* 90:3762–3773.
11. Sanger, J. M., B. Mittal, M. B. Pochapin, and J. W. Sanger. 1987. Stress fiber and cleavage furrow formation in living cells microinjected with fluorescently labeled α-actinin. *Cell Motil. Cytoskeleton.* 7:209–220.

12. Maddox, A. S., L. Lewellyn, A. Desai, and K. Oegema. 2007. Anillin and the septins promote asymmetric ingression of the cytokinetic furrow. *Dev. Cell.* 12:827–835.

13. Kruse, K., J. F. Joanny, F. Jülicher, J. Prost, and K. Sekimoto. 2004. Asters, vortices, and rotating spirals in active gels of polar filaments. *Phys. Rev. Lett.* 92:078101–1.

14. Voituriez, R., J. F. Joanny, and J. Prost. 2006. Generic phase diagram of active polar films. *Phys. Rev. Lett.* 96:028102.

15. Backouche, F., L. Haviv, D. Groswasser, and A. Bernheim-Groswasser. 2006. Active gels: dynamics of patterning and self-organization. *Phys. Biol.* 3:264–273.

16. Smith, D., F. Ziebert, D. Humphrey, C. Duggan, M. Steinbeck, W. Zimmermann, and J. Käs. 2007. Molecular motor-induced instabilities and cross linkers determine biopolymer organization. *Biophys. J.* 10.1529/biophysj.106.095919.

17. Condeelis, J. S., and D. L. Taylor. 1977. The contractile basis of amoeboid movement. *J. Cell Biol.* 74:901–927.

18. Pollard, T. D. 1976. The role of actin in the temperature-dependent gelation and contraction of extracts of *Acanthamoeba*. *J. Cell Biol.* 68:579–601.

19. Ebashi, S., F. Ebashi, and K. Maruyama. 1964. A new protein factor promoting contraction of actomyosin. *Nature.* 203:645–646.

20. Weihing, R. R. 1977. Purification of a HeLa cell high molecular weight actin binding protein and its identification in HeLa cell plasma membrane ghosts and intact HeLa cells. *J. Cell Biol.* 75:95–103.

21. Szent-Györgyi, A. 1945. Studies on muscle. *Acta Physiol. Scand. Suppl. XXV.* 9:1–116.

22. Spicer, S. S. 1951. Gel formation caused by adenosinetriphosphate in actomyosin solutions. *J. Biol. Chem.* 190:257–267.

23. Weber, A., and S. Winicur. 1961. The role of calcium in the superprecipitation of actomyosin. *J. Biol. Chem.* 236:3198–3202.

24. Watanabe, S., and T. Yasui. 1965. The effects of myosin and calcium on the superprecipitation of myosin B. *J. Biol. Chem.* 240:105–111.

25. Stendahl, O. I., and T. P. Stossel. 1980. Actin binding protein amplifies actomyosin contraction, and gelsolin confers calcium control on the direction of contraction. *Biochem. Biophys. Res. Commun.* 92:675–681.

26. Janson, L. W., and D. L. Taylor. 1993. In vitro models of tail contraction and cytoplasmic streaming in amoeboid cells. *J. Cell Biol.* 123:345–356.

27. Janson, L. W., J. Kolega, and D. L. Taylor. 1991. Modulation of contraction by gelation/solation in a reconstituted motile model. *J. Cell Biol.* 114:1005–1015.

28. Kane, R. E. 1983. Interconversion of structural and contractile actin gels by insertion of myosin during assembly. *J. Cell Biol.* 97:1745–1752.

29. Carlsson, A. E. 2006. Contractile stress generation by actomyosin gels. *Phys. Rev. E Stat. Nonlin. Soft Matter Phys.* 74:051912.

30. Ebashi, S., and F. Ebashi. 1965. α-Actinin, a new structural protein from striated muscle. I. Preparation and action on actomyosin-ATP interaction. *J. Biochem.* 58:7–12.

31. Desai, A., A. Murray, T. J. Mitchison, and C. E. Walczak. 1999. The use of *Xenopus* egg extracts to study mitotic spindle assembly and function in vitro. *Methods Cell Biol.* 61:385–412.

32. Pardee, J. D., and J. A. Spudich. 1982. Purification of muscle actin. *Methods Enzymol.* 85:164–181.

33. Margossian, S. S., and S. Lowey. 1982. Preparation of myosin and its subfragments from rabbit skeletal muscle. *Methods Enzymol.* 85: 55–71.

34. Feramisco, J. R., and K. Burridge. 1980. A rapid purification of α-actinin, filamin, and a 130,000-Dalton protein from smooth muscle. *J. Biol. Chem.* 255:1194–1199.

35. Pepe, F. A., and B. Drucker. 1979. The myosin filament. *J. Mol. Biol.* 130:379–393.

36. Liu, J., M. L. Gardel, K. Kroy, E. Frey, B. D. Hoffman, J. C. Crocker, A. R. Bausch, and D. A. Weitz. 2006. Microrheology probes length scale dependent rheology. *Phys. Rev. Lett.* 96:118104.

37. Burlacu, S., P. A. Janmey, and J. Borejdo. 1992. Distribution of actin filament lengths measured by fluorescence microscopy. *Am. J. Physiol. Cell Physiol.* 262:C569–C577.

38. Sakamoto, T., J. Limouze, C. A. Combs, A. F. Straight, and J. R. Sellers. 2005. Blebbistatin, a myosin II inhibitor, is photoinactivated by blue light. *Biochemistry.* 44:584–588.

39. Kaufman, L. J., C. P. Brangwynne, K. E. Kasza, E. Filippidi, V. D. Gordon, T. S. Deisboeck, and D. A. Weitz. 2005. Glioma expansion in collagen I matrices: analyzing collagen concentration-dependent growth and motility patterns. *Biophys. J.* 89:635–650.

40. Kovács, M., J. Tóth, C. Hetényi, A. Málnási-Csizmadia, and J. R. Sellers. 2004. Mechanism of blebbistatin inhibition of myosin II. *J. Biol. Chem.* 279:35557–35563.

41. Raffel, M., C. Willert, and J. Kompenhans. 1998. Particle Image Velocimetry. Springer, Heidelberg, Germany.

42. Kron, S. J., and J. A. Spudich. 1986. Fluorescent actin filaments move on myosin fixed on a glass surface. *Proc. Natl. Acad. Sci. USA.* 83: 6272–6276.

43. Boukellal, H., O. Campás, J. F. Joanny, J. Prost, and C. Sykes. 2004. Soft *Listeria*: actin-based propulsion of liquid drops. *Phys. Rev. E Stat. Nonlin. Soft Matter Phys.* 69:061906.

44. Meyer, R. K., and U. Aebi. 1990. Bundling of actin filaments by α-actinin depends on its molecular length. *J. Cell Biol.* 110:2013–2024.

45. Wachsstock, D. H., W. H. Schwarz, and T. D. Pollard. 1993. Affinity of α-actinin for actin determines the structure and mechanical properties of actin filament gels. *Biophys. J.* 65:205–214.

46. Humphrey, D., C. Duggan, D. Saha, D. Smith, and J. Kas. 2002. Active fluidization of polymer networks through molecular motors. *Nature.* 416:413–416.

47. Katoh, K., Y. Kano, M. Masuda, H. Onishi, and K. Fujiwara. 1998. Isolation and contraction of the stress fiber. *Mol. Biol. Cell.* 9:1919–1938.

48. Tanaka-Takiguchi, Y., T. Kakei, A. Tanimura, A. Takagi, M. Honda, H. Hotani, and K. Takiguchi. 2004. The elongation and contraction of actin bundles are induced by double-headed myosins in a motor concentration-dependent manner. *J. Mol. Biol.* 341:467–476.

49. Miyoshi, H., S. K. Satoh, and E. Y. Y. Hamaguchi. 2006. Temporal change in local forces and total force all over the surface of the sea urchin egg during cytokinesis. *Cell Motil. Cytoskeleton.* 63:208–221.

50. Balaban, N. Q., U. S. Schwarz, D. Riveline, P. Goichberg, G. Tzur, I. Sabanay, D. Mahalu, S. Safran, A. Bershadsky, L. Addadi, and B. Geiger. 2001. Force and focal adhesion assembly: a close relationship studied using elastic micropatterned substrates. *Nat. Cell Biol.* 3:466–472.